

Absolute differential cross section measurements for proton-proton elastic scattering at 647 and 800 MeV[†]

H. B. Willard, B. D. Anderson,* H. W. Baer, R. J. Barrett,[‡] and P. R. Bevington
Case Western Reserve University, Cleveland, Ohio 44106

A. N. Anderson[§] and H. Willmes
University of Idaho, Moscow, Idaho 83543

Nelson Jarmie
Los Alamos Scientific Laboratory, Los Alamos, New Mexico 87545
(Received 19 April 1976)

Absolute differential cross sections for elastic proton-proton scattering have been measured in the center-of-mass angular interval from 20° to 90° at 647 and 800 MeV with overall uncertainties of $\pm(3-10)\%$ and $\pm(3-5)\%$, respectively. The data at 800 MeV are the most accurate so far reported at that energy. Comparison is made to earlier measurements and contemporary phase-shift analyses.

[NUCLEAR REACTIONS ${}^1\text{H}(p, p) {}^1\text{H}$, $E = 647, 800$ MeV; measured $\sigma(\theta)$; $\theta = 23^\circ - 90^\circ$, $\Delta\theta = 3^\circ$.]

I. INTRODUCTION

We report here¹ absolute differential cross sections for proton-proton elastic scattering at 647 and 800 MeV as the first step in our program of experiments at the Clinton P. Anderson Meson Physics Facility (LAMPF) designed to provide a detailed understanding of the proton-proton interaction from 500 to 800 MeV. A similar task^{2,3} has been undertaken at LAMPF for the neutron-proton interaction in this same energy range in order that complete sets of high-precision data be produced for further advances in our knowledge of the nucleon-nucleon force.

The external proton beam (EPB) at LAMPF represents a significant advance over older facilities by virtue of its high intensity, low emittance, small beam size, good energy resolution, and freedom from contamination by other particles. Coupled with the recent developments of multi-wire proportional chambers (MWPC's) and sophisticated on-line data-acquisition systems the high beam quality enabled this experiment to yield data of high precision and accuracy.

Reported measurements of differential cross sections in the energy range of 270–3000 MeV through August 1972 have been compiled by Bystricky, Lehar, and Janout.⁴ Contained therein are some 30 sets of data between 600 and 850 MeV. In addition, new results at 600 MeV have been published by Boschitz *et al.*⁵ and at 726, 751, and 832 MeV and at three lower energies by Abe *et al.*⁶ Much of the earlier data were determined as relative differential cross sections as a func-

tion of either angle or energy. For this reason comparisons of the published results, which often list only the relative uncertainties, with absolute data are sometimes misleading. In this energy range reported measurements with quoted absolute uncertainties of 5%, or better, include Boschitz *et al.*⁵ at 600 MeV, Bogachev and Vzorov⁷ at 657 MeV, Nikitin *et al.*⁸ at 660 MeV, McManigal *et al.*⁹ at 725 MeV, Abe *et al.*⁶ at 726, 751, and 832 MeV, and Neal *et al.*¹⁰ at 831 MeV. Since the energy dependence appears to be smooth and slowly varying, it is possible to make meaningful comparisons of data at slightly different energies.

An energy-dependent phase-shift analysis for proton-proton scattering data from 1 to 500 MeV was published by Arndt, Hackman, and Roper¹¹ which fits the available data above 20 MeV quite well (1233 data points fitted by a solution containing 28 adjustable parameters). An earlier analysis by the Livermore group, MacGregor, Arndt, and Wright,¹² made a fit to data in the region up to 750 MeV, which is handicapped by the sparsity of data in the range above 400 MeV. In addition, the inelastic channels begin to play a more dominant role above 400 MeV and an unique energy-dependent solution must await more accurate and comprehensive experimental results. We indicate in Sec. IV that even the differential cross-section measurements reported here require some adjustment of the Livermore phase shifts. It is well known that the inelastic scattering channel is dominated in this energy region by $\Delta(1236)$ and thus the phase-shift analyses should be sensitive to the imaginary part of the 1D_2 phase for com-

parison with accurate measurements of the differential cross section at 800 MeV.

II. EXPERIMENTAL DETAILS

A floor plan of the experimental arrangement is shown in Fig. 1. The LAMPF external proton beam (EPB) was focused at the target position to a spot size approximately 3 mm in diameter with an emittance less than 1 mr cm. After passing through the target (CH_2 , or C) the beam proceeded some 20 m downstream to the Faraday cup/beam stop. Ion chamber and secondary-emission monitors could also be introduced to intercept the beam about 8 m downstream from the target. The entire beam line was maintained at a vacuum better than 10^{-6} Torr.

The scattering chamber had exit windows of 0.025 mm titanium and 0.051 mm Mylar for the forward and conjugate scattered protons, respectively. Two pairs of multiwire proportional chambers (MWPC's) with wire spacings of 2.5 mm were located 2 m from the target. For some small forward angle runs the conjugate chambers were moved in to 1 m to improve the effective solid angle. The MWPC's were $\sim 16 \times 16 \text{ cm}^2$ and subtended solid angles of 7 msr.

A. Beam characteristics

The LAMPF linac is designed to accelerate simultaneously H^+ and H^- ions, which can then be steered into separate experimental areas (A and B, respectively) after leaving the accelerator.

The energy of the beam has been determined to 1% by measurement $\int \vec{B} \cdot d\vec{l}$ in the deflecting magnets and by comparing the normal deflections in beam bending angle with that produced by the 1.6% change in energy produced by turning off one accelerating module. For the two sets of data reported here the absolute incident beam energies were determined with this accuracy of 1.0% to be 647 and 800 MeV and the energy spread is known to be less than ± 3 MeV. The beam pulses were 350 μs long and 8.34 ms apart (duty factor 4.2%).

The external beam was created by inserting into the H^- beam a thin aluminum foil with a small hole in it. Most of the H^- ions were accordingly stripped and proceeded to the neutron-producing target of the Nucleon Physics Laboratory. The small remaining unstripped portion was separated by bending magnets and became the external proton beam (EPB) with very low emittance (≤ 1 mr cm). The intensity of the EPB was varied from a few picoamperes to tens of nanoamperes (total current of a few microamperes). A triplet of quadrupole magnets allowed the EPB to be focused at any desired location. In our measurements maximum count-rate capabilities of the data-acquisition system limited the beam current to a range from 10 to 300 pA.

B. Beam monitoring

Monitoring of the external beam intensity was carried out with a Faraday cup (FC), an Ar- CO_2 ion chamber (IC), and a secondary-emission

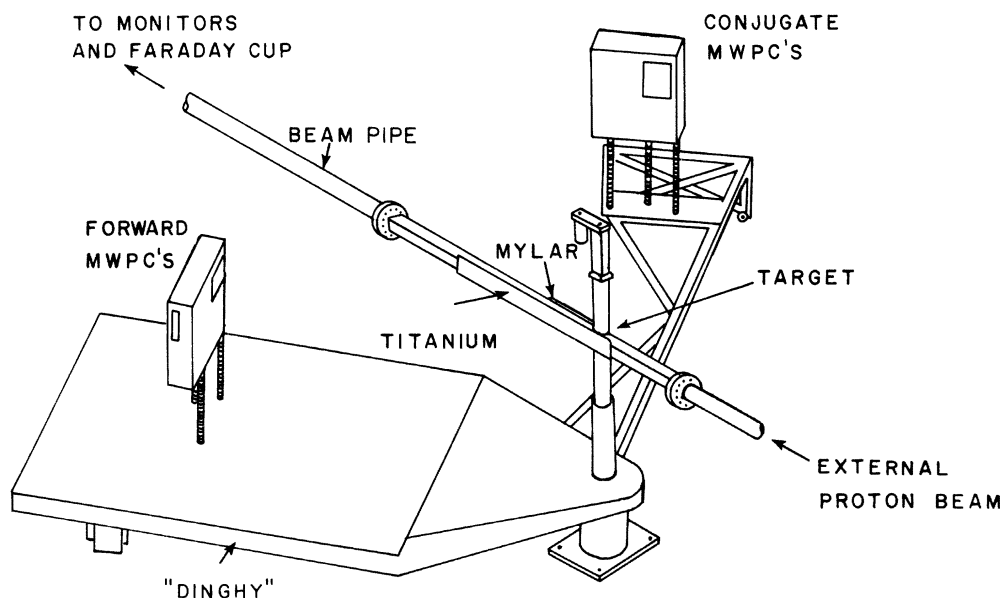


FIG. 1. Floor plan of the experimental arrangement.

monitor (SEM) as reported separately.¹³ The absolute efficiency of the Faraday cup has been measured to be $(99.8 \pm 0.4)\%$ and comparisons with the ion chamber agreed to better than about 2%. The SEM was not satisfactory for the low currents required in these measurements.

The Faraday cup was located in a vacuum vessel 20 m downstream from the target. Charge loss from small-angle deflections due to multiple scattering in the target was minimized by the relatively large 25 cm inner diameter of the reentrant tube in the Faraday cup and the 20 cm diameter vacuum line pipe near the cup. Maintaining the entire cup in the beam line vacuum at 10^{-6} Torr also minimized neutralization of charge on the cup by ions produced in the surrounding gas.

Charge collected from the Faraday cup was conducted 40 m through a coaxial cable to our instrument trailer and integrated there by an Ortec 439 digitizer. The cup was surrounded by a shield connected by a separate cable to ground in the trailer. Precision current sources were connected to the cup to calibrate the system between data runs.

A major problem encountered with the Faraday cup system during the course of this experiment was a negative dark current of up to about 1 pA which appeared intermittently and seemed to correlate with periods of wet weather. It was probably caused by leakage to ground in the long cable from the cup which was exposed to the outside weather conditions. The dark current was small and carefully monitored between runs, but nonetheless prevented achievement of the highest inherent absolute precision of the Faraday cup. As discussed below, our quoted overall uncertainties in normalization were thereby increased.

C. Targets

Target foils of polyethylene (CH_2) and carbon approximately 2.5 cm square were mounted on a holder and bombarded by the EPB. In addition to the several targets, a phosphor screen was mounted in one of the positions for monitoring the beam spot size and location. Although the CH_2 targets increased the background from quasi-elastic scattering, the ease of handling and the improved kinematic precision of locating forward and conjugate scattered protons were deemed sufficient compensation over the alternate choice of a liquid hydrogen target.

The thickness of each CH_2 target was measured at several positions on a Pratt and Whitney super micrometer with an 8 oz pressure anvil 1 cm in diameter. The size of the anvil and the pressure limitation prevented deformation of the polyethyl-

ene during measurement. Gradual variations in thickness of a few percent were observed across each target. The stated thickness and uncertainty were taken from measurements of the center square centimeter where the beam was constrained to strike.

Three CH_2 targets with thicknesses of 3.43 ± 0.05 , 10.18 ± 0.04 , and 18.71 ± 0.10 mg/cm² were bombarded.

In order to measure the background contribution from quasielastic scattering a machined pyrolytic carbon foil of thickness (determined by weighing) 12.79 ± 0.11 mg/cm² was also bombarded.

D. Multiwire proportional chambers

The design and operating characteristics of our multiwire proportional chambers (MWPC's) have been described elsewhere.¹⁴ These chambers have an active area of 16×16 cm² with anode wires of 20 μm gold plated tungsten spaced 2.5 mm apart epoxied to frames of copper clad 3 mm G-10 plastic. Cathode planes of 6.35 μm aluminized Mylar (aluminum sides toward the anode) were located 4.76 mm on either side of the anode plane. A gas mixture of 55% argon, 35% isobutane, 10% methylal (di-methoxymethane), and 0.3% freon circulated freely throughout the chambers which were sealed on the outer frame with 0.006 mm clear Mylar windows located 3 mm beyond each cathode plane. The gas flow rate was about 50–100 cm³ per minute. The methylal concentration was controlled by maintaining the temperature at $(29 \pm 2)^\circ\text{F}$. High voltage settings of 3.3 to 3.8 kV typically produced absolute chamber efficiencies between 95 and 98%. The X and Y planes were separate detectors which allowed for additional freedom in logic gate requirements.

E. Data acquisition

A digital readout system for the MWPC's was developed¹⁵ expressly for this series of experiments on proton-proton scattering at medium energy. The primary criterion for design was speed of response, including fast recovery from extraneous events, parallel encoding of multiple events, and buffering to minimize effective dead time.

Electronics logic at the MWPC detector includes a threshold comparator and flip-flop buffer for each wire and a serial-parallel encoder which strobes the buffer serially to locate up to three separate simultaneous events and encodes the buffer in parallel into corresponding binary addresses. Threshold levels were set at 20 mV, and all inputs for any MWPC were disabled 90 ns after detection of an event by that MWPC to minimize multiple firing on a single event.

A coincidence trigger NIM module provides selection of two alternate patterns of MWPC's for coincidence criteria, either of which must be satisfied by an event to initiate storage and analyzing. For this experiment the criteria consisted of the EPB "on" pulse (indicating presence of the beam on target) and either both "X" or both "Y" MWPC's. Resolving time for coincidence overlap was set at 160 ns; the maximum time difference measured between forward and conjugate proton detection was 22 ns with a jitter of ± 20 ns on each.

Events which satisfy the coincidence requirements have their addresses encoded and stored in input register CAMAC modules. The total time for acquisition, coincidence, encoding, and transfer was about $1 \mu\text{s}$, including delay in cable transmissions, after which the detector and coincidence logic are free to accept and test new events. Data in the input registers, plus a check-word (indicating which MWPC's detected events) accumulated in a master control CAMAC module, are transferred (in about $20 \mu\text{s}$) to a buffer in the CAMAC microprogrammed branch driver (MBD¹⁶) and from thence through priority interrupt to a PDP-11/45 computer for storage on magnetic tape and reduction for real-time graphic control.

Dead time is determined by monitoring the enabling input to the flip-flop buffer at each detector. Each buffer is disabled shortly (60 ns) after an event is detected by its own MWPC, or as soon as coincidence criteria for all MWPC's are met, and it is enabled again after the coincidence resolving time (160 ns) for an event that does not satisfy coincidence criteria, or after transfer of addresses to all CAMAC input registers is complete ($1 \mu\text{s}$). Pulses from the ion-chamber digitizer (which is correlated with the beam, but not correlated with individual events) strobe the enabling input to determine what fraction of the beam is ignored by the detectors. The effect of dead time was not significant.

F. On-line data monitoring

Between events the computer accumulated and displayed histograms of chamber counts and distributions in the opening angle $\Delta\theta$ and coplanarity $\Delta\phi$. The former histograms allowed each chamber to be continuously monitored for bad wires, noisy spots, and relative inefficiencies.

III. DATA REDUCTION

The number of protons $N_s(\theta)$, scattered at angle θ into an interval of solid angle $\Delta\Omega$, with energy spread ΔE , by a target of n_t protons per cm^2 is related to the total number of incident protons N_i by the differential cross section for elastic scat-

tering $\sigma(\theta, E)$ in the usual way:

$$N_s(\theta) = N_i n_t \overline{\sigma(\theta, E) \Delta\Omega},$$

where the cross section average is taken over the finite-energy and solid angle intervals set by the experimental conditions. The measurements of all parameters required to calculate the differential cross section together with the appropriate corrections are discussed in the following subsections.

A. Incident beam intensity N_i

The absolute beam intensity was measured directly with the Faraday cup and monitored with the ion chamber as a secondary standard. Although as reported elsewhere¹³ this Faraday cup has an inherent absolute accuracy of better than 1%, we were troubled during the experimental runs with charge leakage in the coaxial cables which increased the uncertainties associated with this parameter in some cases to much larger values (10% in the worse case). Only measurements where the ion chamber and Faraday cup agreed to better than $\pm 2\%$ were included for the final results reported here.

The Faraday cup, coaxial cables, and current digitizer were calibrated frequently during the runs with a Keithley picoampere source and a precision current source accurate to $\pm 0.1\%$ that ranged down to 15 nA. After correcting for the secondary electron emission and charge leakage in the Faraday cup (-0.4%), the overall absolute determination of N_i is conservatively rated to have an uncertainty of $\pm 3\%$ for all accepted measurements. Multiple scattering of the beam introduced by the thickest CH_2 target and the ion chamber did not exceed an rms radius of 1 cm at the Faraday cup (entrance aperture 25 cm diam).

B. Target thickness n_t

The composition and target thickness determination have already been discussed in Sec. IIC. The only additional contributions to the uncertainty in n_t result from the target orientation and hydrogen loss due to heating by the incident beam.

For runs at laboratory angles of 25° and larger the targets were positioned normal to the beam. The 4° uncertainty in setting target angles yields less than 0.25% additional uncertainty in the target thickness. At scattering angles smaller than 25° the targets were rotated about a vertical axis to be at 45° toward the conjugate chambers to minimize multiple scattering effects in this system. The target angle setting was determined to within 0.05° by recording the position of a radius arm affixed to the target holder. For these runs the additional

uncertainty in target thickness was less than 1%. For some early runs where the target angle was not measured with sufficient precision, subsequent evaluation yielded an estimated additional uncertainty up to a maximum of 3%.

The passage of 800 MeV protons through the target resulted in energy deposition of 2.5 MeV cm²/g in the target. This ionization energy liberated H atoms which could then diffuse out of the target as H₂ gas. At 100 pA of proton beam with a 1 mm radius this effect could cause a release H₂ at a rate of about 0.01% per hour.¹⁷ For these measurements calculations indicate that a maximum correction of $(-0.5 \pm 0.5)\%$ to our target thickness n_t is required.

C. Solid angle $\Delta\Omega$

The solid angle interval $\Delta\Omega$, within which the elastically scattered protons were to be counted, was determined by setting windows (numbers of wires) on the forward (X1, Y1) chambers such that every proton conjugate to one scattered elastically into the interval would be sure to strike the conjugate pair of chambers. These windows were determined empirically by inspection of the event distributions in the forward detectors. The uncertainty in solid angle is due chiefly to the variation across the detectors in wire spacing.

The optimum solid angle chosen for these measurements represents a trade-off between the improvement in statistical precision of a large interval vs angular resolution of a small one. The possible choices ranged from an angular interval of 3° (lab) with 0.7% statistics and 0.08% solid angle uncertainty (20 000 events over 42 wires) to 0.07° (lab) with 5% statistics and 3% solid angle uncertainty (500 events on one wire). All available information suggests that there is no measurable structure in the cross section over 3° and this interval was adopted for the final results.

D. Number of scattered protons $N_s(\theta)$

Proton-proton elastic scattering is two body in its final state which means that there is a definite and unique opening angle between the forward and conjugate scattered protons and a requirement that their trajectories be co-planar with the incident beam. The addresses of the detector wires can be used to identify protons satisfying both these requirements, and by calculating the deviations from these proper values of a two-dimensional histogram can be constructed for all events detected in both the forward and conjugate pairs of MWPC's. The deviation from the proper opening angle $\Delta\theta$, and the deviation from coplanarity $\Delta\phi$, are shown in Fig. 2. The expected concentration of elastic

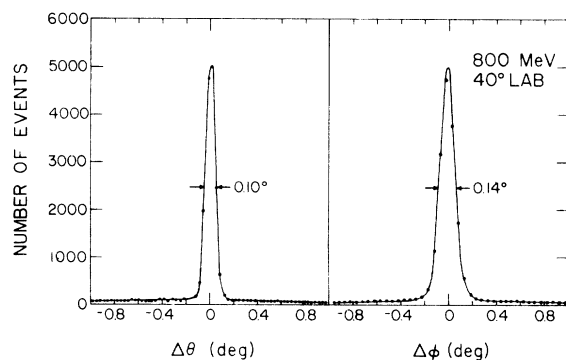


FIG. 2. Typical histograms of events in $\Delta\theta$ and $\Delta\phi$ for a run at 40°, 800 MeV.

events near the center of the target is evident, while inelastic and carbon quasielastic scattering events show essentially a random distribution in the $\Delta\theta$ - $\Delta\phi$ plane. The very sharp peak with relatively small background results from the combination of high spatial resolution of the MWPC's and the small spot size and emittance of the beam. The ratio of elastic to background events is much larger than for any of the earlier published p - p elastic-scattering differential cross-section measurements. Errors in either the horizontal position of the conjugate detectors or the beam elevation appeared as shifts in the position of the elastic peaks in $\Delta\theta$ or $\Delta\phi$, respectively. The finite widths of the narrow peaks are due primarily to multiple Coulomb scattering in the air between the scattering chamber and the detectors.

Most of the background due to inelastic and quasielastic scattering can be excluded by the kinematic criteria. A separate background measurement was made with the carbon target at several angles and a Monte Carlo program was written to simulate the background assuming a uniform random distribution of events in the four chambers. The real and generated backgrounds agreed very well; therefore the Monte Carlo calculation was used for all background subtractions. Typical backgrounds constituted from 0.5 to 5% of the elastic peak area. Uncertainties in these background determinations are shown in Table I.

The number of detected events must be corrected for detector inefficiencies, dead time, displaced events, logic inefficiency, and multiple scattering. The "OR" coincidence requirement allowed the recovery of all events in which only one of the four chambers failed to fire. Inspection of the checkword for each event allowed statistics to be compiled for each detector from which its actual efficiency during the run could be calculated. The inefficiency of each chamber was taken as the percent of counts not seen by that chamber when all

TABLE I. Typical uncertainties.

N_i , Incident beam intensity	
Faraday cup/ion chamber	$\pm(2-3)\%$
n_t , target thickness	
Direct measurement	$\pm(0.5-1.5)\%$
Angle setting	$\pm(0.3-1.0)\%$
Hydrogen loss	$\pm(0.5)\%$
Subtotal (rms)	$\pm(0.8-2.0)\%$
$\Delta\Omega$, solid angle	
Number of effective wires	$\pm(0.2-0.3)\%$
$N_s(\theta)$, number of scattered protons	
Counting statistics	$\pm(1.0-2.6)\%$
Background subtraction	$\pm 0.5\%$
Counter efficiency	$\pm 0.5\%$
Displaced events	$\pm(0.5-2.8)\%$
Dead time	$\pm(1.0-2.0)\%$
Multiple scattering	$\pm(1.0-3.0)\%$
Subtotal (rms)	$\pm(1.6-4.6)\%$
$\sigma(\theta, E)$, Differential cross section	
Total (rms)	$\pm(2.8-6.4)\%$

three other chambers did trigger. Constraints on the wire locations in the other three chambers were imposed to ensure that the particle must have traversed the chamber of interest. Typical fourfold coincidence inefficiencies varied between 2 and 7% and were determined to be better than 0.5%. Loss of elastic events was possible from accidental coincidences with other elastic and quasielastic events as well as from the much larger background flux due to inelastically scattered protons, pions, and electrons. Although the dead time meter monitored these effects by sampling the read-inhibit level of each chamber, the correction was complicated by the timing and logic of the data-acquisition system. A detailed discussion of this correction is available.¹⁸ Typical dead times ranged from 2.0 to 2.5% with uncertainties in this correction of 1.0 to 2.0%.

Some events were displaced from their proper kinematic addresses by accidental coincidences, or by detection of scattered electrons (δ rays). A correction of from 2 to 5%, with uncertainties about half the size of the correction was made to all measurements because the logic did not read out more than one wire location in each chamber even if the two wires were triggered simultaneously. An additional uncertainty was introduced from Coulomb multiple scattering in the target, scattering chamber windows, air flight path, and the detectors. This affects the determination of the elastic peak areas in two ways. First, protons can be multiple scattered outside the chambers and thereby lost, and, second, they can be scattered

outside the elastic peak and misinterpreted as background. A theoretical correction, generally negligible, was made. Somewhat larger corrections were made for the 647 MeV data at 10 and 15° (lab) [(3±3)% and (1±1)%, respectively].

Logic inefficiency of the output from the coincidence flip-flop was monitored by a scaler which allowed comparison with the number of events recorded on tape. This comparison shows typically a loss of less than 0.5%, of which most events probably did not involve an elastic event.

The number of scattered protons $N_s(\theta)$, was corrected for all effects discussed in this section. The overall uncertainty in N_s was typically about ±2%, including statistics.

E. Rejection of data runs

Only about one-third of the experimental runs are included in our final results. In addition to the beam normalization problem, criteria for rejection included measurements taken with improper beam location, runs with anomalously high backgrounds resulting in large uncertainties in N_s , and low detector efficiencies (below 95%) for any one detector. In general, the standard deviation of the acceptable runs, weighted for their respective uncertainties (external variance), should be less than or equal to the weighted mean of the calculated uncertainties (internal variance). Any difference is attributed to (unknown) systematic errors in the measurement. The larger of the two uncertainties is quoted in the final results (Table II) for each energy and angle.

Table I summarizes typical contributions to the calculated uncertainties.

IV. RESULTS AND DISCUSSION

Values for the absolute differential cross section for proton-proton elastic scattering at 647 and 800 MeV are presented in Table II. Comparison with calculations based on the phase-shift analysis of MacGregor, Arndt, and Wright¹² are shown in Figs. 3 (647 MeV) and 4 (800 MeV) and discussed further below.

With some exceptions the results of this experiment (accurate to 3–5% absolute at 800 MeV and 3–10% absolute at 647 MeV) agree with previous measurements within the stated uncertainties, after making allowance for possible normalization errors in relative measurements. That these measurements at 800 MeV are more accurate than earlier results is due, primarily, to three features of the present experiment. First, the external proton beam at LAMPF has characteristics which are nearly perfect for this type of experiment. The second condition was the use of MWPC's with

TABLE II. Measured differential cross sections for proton-proton elastic scattering.

Energy (MeV)	$\theta_{\text{lab}} \pm \Delta\theta_{\text{lab}}$ (deg)	$\sigma_{\text{lab}}(\theta) \pm \Delta\sigma_{\text{lab}}(\theta)$ (mb/sr)	$\theta_{\text{c.m.}} \pm \Delta\theta_{\text{c.m.}}$ (deg)	$\sigma_{\text{c.m.}}(\theta) \pm \Delta\sigma_{\text{c.m.}}(\theta)$ (mb/sr)
647	10.1 ± 0.6	36.6 ± 1.6	23.3 ± 1.3	7.06 ± 0.30 (4.3%)
	14.9 ± 0.8	27.1 ± 1.1	34.3 ± 1.8	5.45 ± 0.21 (3.9%)
	19.8 ± 1.0	18.90 ± 0.45	45.3 ± 2.1	4.04 ± 0.10 (2.4%)
	24.9 ± 0.9	14.00 ± 0.95	56.6 ± 2.0	3.23 ± 0.22 (6.8%)
	29.8 ± 1.0	9.95 ± 0.34	67.2 ± 2.1	2.51 ± 0.09 (3.4%)
	34.8 ± 1.5	7.47 ± 0.73	77.7 ± 3.1	2.09 ± 0.20 (9.8%)
	39.9 ± 1.5	6.06 ± 0.34	88.2 ± 3.0	1.91 ± 0.11 (5.6%)
800	9.8 ± 0.8	46.3 ± 2.2	23.3 ± 1.9	8.44 ± 0.40 (4.8%)
	15.0 ± 0.8	30.0 ± 1.5	35.5 ± 1.8	5.76 ± 0.26 (5.1%)
	20.0 ± 0.9	19.55 ± 0.88	47.0 ± 2.1	4.02 ± 0.18 (4.5%)
	24.9 ± 1.0	11.55 ± 0.27	58.0 ± 2.1	2.58 ± 0.06 (2.3%)
	29.9 ± 1.5	6.26 ± 0.21	69.0 ± 3.2	1.55 ± 0.05 (3.4%)
	34.9 ± 1.1	4.11 ± 0.13	79.6 ± 2.2	1.14 ± 0.04 (3.2%)
	39.9 ± 1.5	3.15 ± 0.10	89.9 ± 3.0	0.994 ± 0.030 (3.3%)

their excellent spatial resolution which allowed for such a high ratio of elastic events to the quasi-elastic background. Finally, the development of the 1700 kg Faraday cup allowed for the most accurate charge integration of medium-energy proton beams to date. That the results were not

quite as accurate as may ultimately be possible with this system was due primarily to the fact that this was one of the first experiments on this beam line and many problems were discovered during the running and analysis.

The present measurements at 647 MeV were

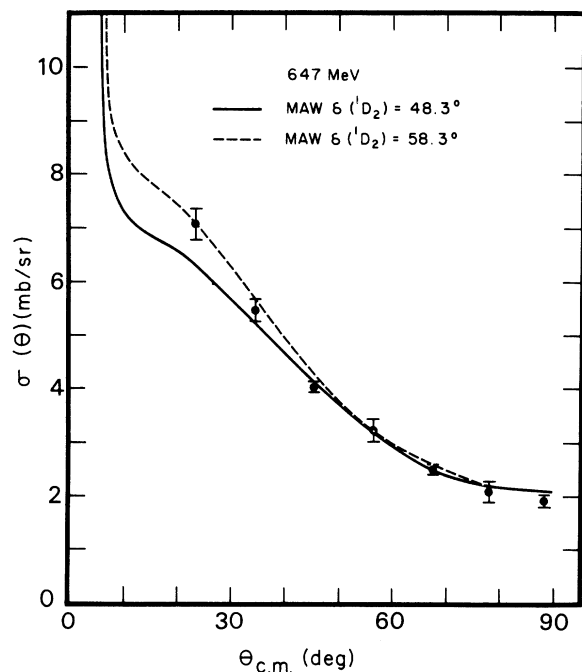


FIG. 3. Comparison of the results of this experiment at 647 MeV with calculations (solid line) based on the phase-shift analysis of MacGregor, Arndt, and Wright (Ref. 12). The dashed line was obtained by increasing the imaginary component of the singlet $D(S=0, J=2)$ phase shift by 10° (from 48.3° to 58.3°).

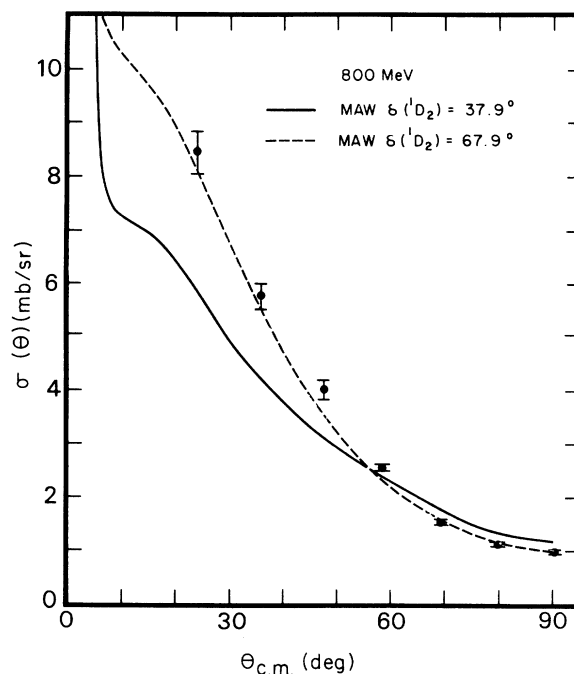


FIG. 4. Comparisons of the results of this experiment at 800 MeV with calculations (solid line) based on the phase-shift analysis of MacGregor, Arndt, and Wright (Ref. 12). The dashed line was obtained by increasing the imaginary component of the singlet $D(S=0, J=2)$ phase shift by 30° (from 37.9° to 67.9°).

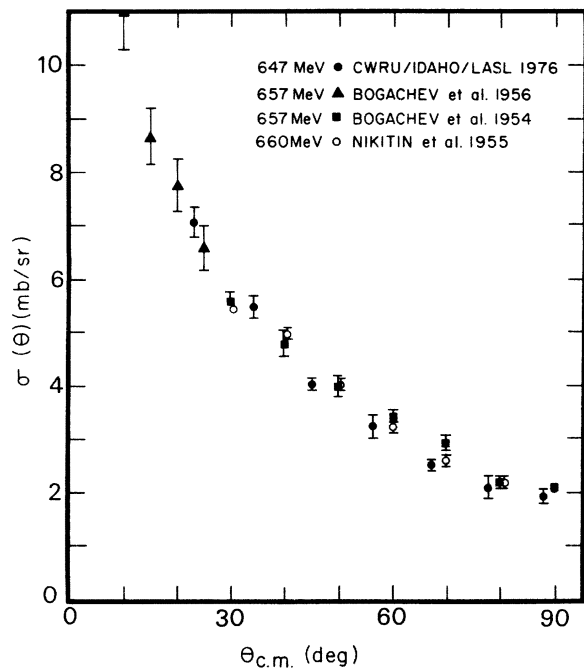


FIG. 5. Comparison of the results of this experiment at 647 MeV with other absolute measurements (Refs. 7 and 8) in this energy region.

limited in absolute accuracy due to the Faraday cup problems discussed in Sec. IIB and the reduced availability of accelerator time at this energy. Nonetheless, the overall uncertainties are comparable, or better than, the best previous absolute measurements in this energy region, i.e., those of Bogachev and Vzorov⁷ and Nikitin *et al.*⁸ The agreement among all three sets of data is quite within the typical uncertainties of 2–6% as seen in Fig. 5.

The Livermore phase-shift analysis,¹² shown as a solid line in Fig. 3, fits our data quite well except for the most forward two angles. Increasing the imaginary component of the 1D_2 phase shift by 10° (from 48.3° to 58.3°), shown as the dashed line in Fig. 3, improves the fit considerably.

At 800 MeV we were able to achieve overall absolute uncertainties from 2–5%, which make the data the best available. The recent high-quality measurements by Abe *et al.* at 751 and 832 MeV have absolute uncertainties from 3 to 6% and, allowing for the slight energy variation, bracket our results nicely. Measurements by Neal *et al.*¹⁰ have quoted uncertainties of 2–3%. Agreement between all three sets of data, shown in Fig. 6, is quite good in the region of 60° – 90° c.m., but the data begin to diverge near 50° c.m. with the 831 MeV data of Neal *et al.*¹⁰ some 20% higher at 47.6° c.m. (their most forward angle). Ryan *et al.*¹⁹ have reported measurements at 789 MeV with

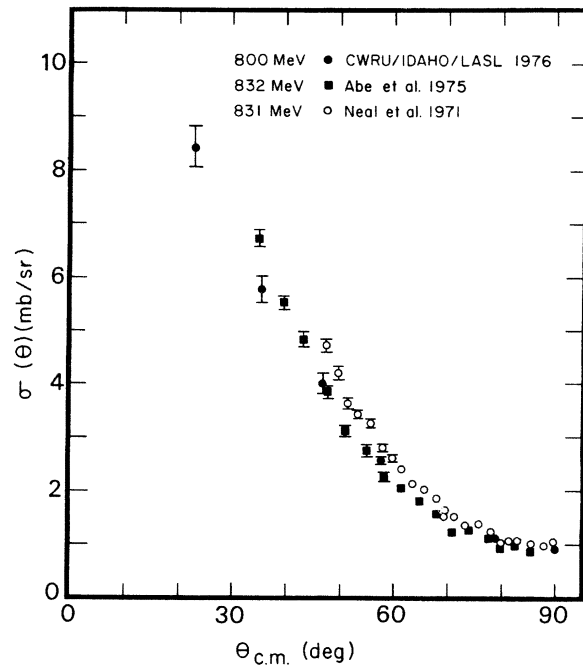


FIG. 6. Comparison of the results of this experiment at 800 MeV with other absolute measurements (Refs. 6 and 10) in this energy range.

overall uncertainties in the range 8–20%. Disagreement with our results and those of Abe *et al.*⁶ is beyond the stated uncertainties. Perhaps this is due to the large normalization correction they¹⁹ were forced to make ($\sim 50\%$).

An extrapolation of the Livermore phase shifts to 800 MeV is shown as a solid line in Fig. 4. At this energy the divergence from our data increases rapidly below 60° c.m. The fit is considerably improved by increasing the imaginary part of the 1D_2 phase shift by 30° (from 37.9° to 67.9°) as shown by the dashed line in Fig. 5. Changes in the 3P or 3F imaginary phase shifts increased the cross sections overall, worsening the fits at large angles. It should also be noted that the total elastic cross sections calculated with the larger 1D_2 imaginary phase shifts are in better agreement with experimental data. At 647 MeV the calculated total cross section increases from 35.2 to 37.9 mb compared with the experimental value of 40 mb. At 800 MeV the calculated cross section increases from 32.9 to 39.3 mb compared with the experimental value of 48 mb.

Special thanks are due Frank Cverna, who aided in the construction of the wire chambers and particularly in the data acquisition, to Bob Leskovec and Larry Hinkley, who provided technical support, and to Louis Rosen, Don Hagerman, Lewis Agnew, and the members of the LAMPF staff who provided assistance and support during the running of this experiment.

- [†]Work supported in part by the Energy Research and Development Administration.
- *Present address: Physics Department, Kent State University, Kent, Ohio 44242.
- [‡]Present address: Los Alamos Scientific Laboratory, Los Alamos, New Mexico 87545.
- [§]Present address: Physics Department, University of Alberta, Edmonton, Alberta, Canada T6G-2E1.
- ¹Preliminary results were presented at the Sixth Conference on High Energy Physics and Nuclear Structure, Sante Fe, June 9-14, 1975 [Los Alamos Report No. LA-6030-C (unpublished), p. 252].
- ²L. C. Northcliffe, M. L. Evans, G. Glass, J. C. Hiebert, M. Jain, H. D. Bryant, C. Cassapakis, S. Cohen, B. D. Dieterle, D. M. Wolfe, B. E. Bonner, J. E. Simmons, D. Werren, C. W. Bjork, P. J. Riley, in Proceedings of the International Conference on Few Body Problems in Nuclear and Particle Physics, Laval 1975 (unpublished), p. 134.
- ³J. E. Simmons, in Proceedings of the Sixth International Conference on High Energy Physics and Nuclear Structure, Sante Fe, June 9-14, 1975 (see Ref. 1), p. 103.
- ⁴J. Bystricky, F. Lehar, and Z. Janout, Saclay Report No. CEA-N-1547 (E), 1972 (unpublished).
- ⁵E. J. Boschitz, W. K. Roberts, J. S. Vincent, M. Blecher, K. Gotow, P. C. Gugelot, C. F. Perdrisat, L. W. Swenson, and J. R. Priest, Phys. Rev. C 6, 457 (1972).
- ⁶K. Abe, B. A. Barnett, J. H. Goldman, A. T. Laasansen, P. H. Steinberg, G. J. Marmar, D. R. Moffett, and E. F. Parker, Phys. Rev. D 12, 1 (1975).
- ⁷N. P. Bogachev and I. K. Vzorov, Dokl. Akad. Nauk SSSR 99, 931 (1954); N. P. Bogachev, Dokl. Akad. Nauk SSSR 108, 806 (1956) [Sov. Phys. Dokl. 1, 361 (1956)].
- ⁸S. Ya. Nikitin, Ya. M. Selector, E. G. Bogomolov, and S. M. Zombkovski, Nuovo Cimento 2, 1269 (1955).
- ⁹P. C. McManigal, R. D. Eandi, S. N. Kaplan, and B. J. Moyer, Phys. Rev. 137, B620 (1965).
- ¹⁰H. A. Neal, B. B. Brabson, R. R. Critenden, R. M. Heinz, R. C. Kammerud, H. W. Paik, and R. A. Sidwell, Indiana University Report No. COO-2009.15, 1971 (unpublished).
- ¹¹R. A. Arndt, R. H. Hackman, and L. D. Roper, Phys. Rev. C 9, 555 (1974).
- ¹²M. H. MacGregor, R. A. Arndt, and R. W. Wright, Phys. Rev. 169, 1149 (1968).
- ¹³R. J. Barrett, B. D. Anderson, H. B. Willard, A. N. Anderson, and N. Jarmie, Nucl. Instrum. Methods 129, 441 (1975).
- ¹⁴P. R. Bevington, B. D. Anderson, F. H. Cverna, R. J. Barrett, and A. N. Anderson, Nucl. Instrum. Methods 129, 373 (1975).
- ¹⁵P. R. Bevington and R. A. Leskovec (unpublished).
- ¹⁶BiRa Systems, Inc., Albuquerque, New Mexico.
- ¹⁷A. Chapiro, *Radiation Chemistry of Polymeric Systems* (Interscience, New York, 1962).
- ¹⁸A. N. Anderson, University of Idaho, Ph.D. dissertation, 1975 (unpublished).
- ¹⁹B. A. Ryan, A. Kanofsky, T. J. Devlin, R. E. Mischke, and P. F. Shepard, Phys. Rev. D 3, 1 (1971).